LASER TUBE CUTTING - THROAT AND STRESS DISTRIBUTION IN CHS-to-CHS JOINTS WELDED BY PARTIAL JOINT PENETRATION (PJP) ACCORDING TO EN9692, AS/NZS1554 AND AWS-D1.1

AUGUSTO MASTROPASQUA[1] LUCA SPORTELLI[2]

SERGIO RASO[3] CLAUDIO DUARTE[4]

[1]MZA Research - Numerical Consulting, 4-12 Regent Street, SW1Y 4PE London, UK
E-mail: research@mza-structuralengineering.com
[2]Faculty of Engineering Technology, EGS University, 75000 Paris, France
E-mail: info@egs.education
[3]CMM Laser, 46046 Mantova, Italy
E-mail: info@cmmlaser.it
[4]ARUP, 10 High St, Melrose Arch, Johannesburg, 2076, South Africa
E-mail: claudio.duarte@arup.com

With the latest technological advancements in the field of tubular laser cutting, new robotic systems have been introduced into the industry enabling a host of new opportunities for laser cutting. Over the past decade, the manufacturers of the most advanced laser-cutting machinery have made significant breakthroughs in the CNC (computer numerical control) field, by utilizing the efficiency of the reversible laser-beam (multi-axis robotic system). In this paper, the CNC approach is used to provide a full set of geometric commands that mathematically govern the continuous variation in the PJP post-bevelled dihedral angle along the intersection path of the CHS-to-CHS joint. This enables the establishment of the size, position and spatial inclination of the throat-plane along the welded path, allowing the authors the opportunity to effect a representative finite element model to simulate the real stress distribution through the welded region (WR) and the nominal throat-plane (TP) surface. The study culminates with the completion of the experimental phase aimed at obtaining 5 samples that are wholly compatible to the EN(ISO)9692, AS/NZS1554 and AWS-D1.1 welding codes.

Keywords: Tubular joints, tubular structures, laser tube technology, welding.

1 Introduction

In this work, welded tubular connections are studied with explicit reference to the new end-machining possibilities offered by the Laser-Tube-Cutting technology (LTC). The particular case of the circular hollow section (CHS) is dealt with, thus referring to the class of connections typically referred to as CHS-to-CHS. Special emphasis is placed on the role of the 3-dimensional digital design possible nowadays, thanks to the improvement of the CAD and CAM technology. The geometrical complexity, which inherently characterizes the CHS-to-CHS intersection, has been modelled here in terms of the mathematical shape of the joint, providing the exact spatial distribution and the correct identification of the throat-plane and size, which generally applies to fillet welds (FW), partial joint penetration (PJP) and compound joint penetration (FW+PJP) solutions. A new methodology in terms of the design and end-machining of CHS-to-CHS tubular

Proceedings of the 17th International Symposium on Tubular Structures.
Editors: X.D. Qian and Y.S. Choo

Published by Research Publishing, Singapore.
ISBN: 978-981-11-0745-0; doi:10.3850/978-981-11-0745-0_028-cd

intersections welded by partial joint penetration (PJP) is introduced, where the bevel-surface is wholly governed along its path from the design (3D-CAD) to the execution (3D-CAM) by a digital approach. An experimental phase aimed at obtaining 5 samples of tubular intersections, by making use of 2 of the most advanced laser-tube cutting machines available, was conducted. The samples were obtained thanks to the CMM LASER (Italy), using a last-generation model of 6-axis CO_2 laser machine produced by Mazak Optonics Corp (Japan). The optimal setting of the lasers power level, pulse mode, focal length, focal point and cutting speed all result in a very precise 3D bevelled-surface, with a clear identification of the throat plane (TP) along the welded path. This, allowed for a non-linear numerical finite element analysis to be developed to investigate the mechanical response of the PJP solution, and its advantages in terms of stress and ultimate strength on the classic FW solution.

2 Fillet weld (FW) and partial joint penetration (PJP) solution in CHS-to-CHS joints: the throat-thickness geometric efficiency factor (χ_{at})

Illustrations of the weld regions for FW joints have been indicated in Figures 1, 2 and 3 respectively, for obtuse (ψ>90°deg), right-neutral (ψ=90°deg) and acute (ψ<90°deg) dihedral angles. These three-potential geometric configurations are generally applicable to a CHS-to-CHS intersection where the welded path moves from the crown point of the connection, through the saddle point to the heel point. In Figures 1 to 3, the parameter $g_{1.geom}$, represents the *geometrical gap,* which directly results from the dihedral angle (ψ) and the brace wall-thickness (t_1), therefore $g_{1.geom} = g_{1.geom}(\psi,t_1)$. However, the initial *assembly gap*, also referred to as $g_{1.ass}$ and indicated by EN9692, AS/NZS1554 and AWS-D1.1, should also be taken into account.

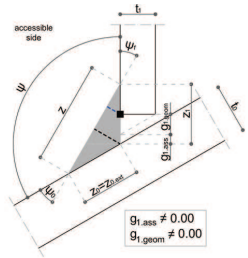

Figure 1. FW, obtuse angle

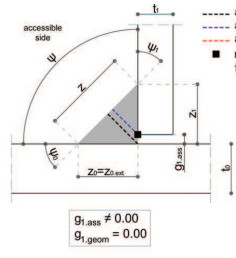

Figure 2. FW, neutral angle

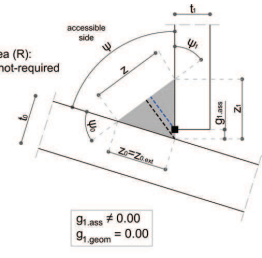

Figure 3. FW, acute angle

It should be noted that $g_{1.ass}$ represents a fundamental parameter in the characterization of the welded joint; it can typically be introduced in the welded connection as result of the workshop assembly procedure for several reasons; member length tolerance, thermal expansion tolerance, thermal-distortion tolerance and accidental (geometric) error during the assembly phase. It thus follows that the $g_{1.tot}$ parameters should be correctly addressed during the design phase, especially for the throat-assessment phase, by means of Equation 1. Equation 2, however, introduces the *throat-thickness geometric efficiency factor*, as a parameter which can provide a comparison between the effective throat dimension (governed by the dimensional parameter a_{eff}) and the brace wall-thickness (t_1).

$$g_{1.tot} = g_{1.tot}(\psi,t_1) = g_{1.ass} + g_{1.geom}(\psi,t_1) \quad (1)$$

$$\chi_{at} = \chi_{at}(\psi,t_1,\beta_1,g_{1.ass}) = a_{eff}/t_1 \quad (2)$$

Now, assuming that in Figures 1 to 3, z is the external (visible) side of the weld region, z_0 and z_1

as the chord-side and brace-side of the weld region, t_1 as the brace wall-thickness, ψ as the dihedral angle between the welded walls, ψ_0 as the chord-angle and ψ_1 as the brace-angle of the weld region, a as the nominal throat of the weld region, a_{eff} as the effective throat of the weld region, assuming $g_{1.ass}$ = 0.00 mm for simplicity, and considering therefore t_1, z_0, z_1, as independent variables, the χ_{at} distribution is visible in Figures 4 to 7. The brace wall-thickness was assumed t_1=8.00 and 15.00 mm, the visible-inspection parameter z_0 was assumed 5.00 and 7.00 mm (for the case t_1=8.00 mm) and 7.00, 10.00 mm (for the case t_1=15.00 mm), where $r=z_0/z_1$ was varied between 0.50 and 1.50 and the dihedral angle has been varied from 30° to 150°deg (i.e. $\psi = 90^{\pm 60}$).

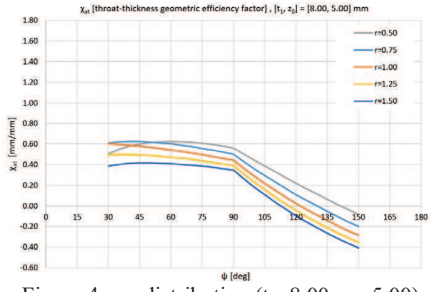

Figure 4. χ_{at} distribution (t_1=8.00, z_0=5.00)

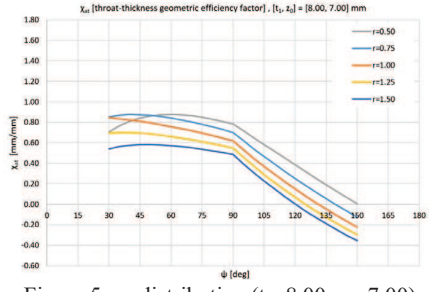

Figure 5. χ_{at} distribution (t_1=8.00, z_0=7.00)

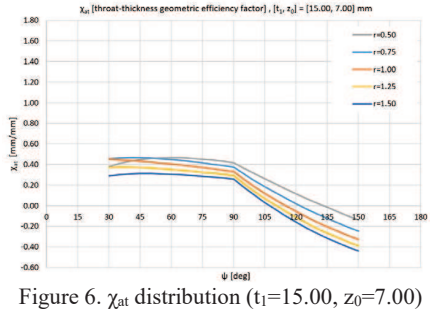

Figure 6. χ_{at} distribution (t_1=15.00, z_0=7.00)

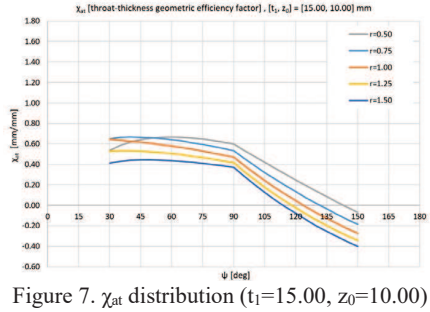

Figure 7. χ_{at} distribution (t_1=15.00, z_0=10.00)

It should be noted that of the 4 throat-distributions that have been represented above, these make up only an individual case of an extensive database, listed in Mastropasqua (2019), where a comprehensive case study utilizing the current tubular sections that are typically adopted in the field of architecture and light industrial structures have been covered. The 4 distributions that have been covered here, however, were done so as they highlight some interesting and generalizable considerations: although continuous in the range $\psi \epsilon [30,150]$°deg, negative values of a_{eff} are observed when ψ approaches to acute dihedral angles ($\psi \rightarrow 150$°deg), clearly indicating geometrical inconsistencies of the welded region on the external side of the brace wall thickness. However, due to the pure geometric nature of the study, negative values of χ_{at} should be ignored, as indicating this is meaningless in the sense of physically achieving these types of weld. Now, considering the PJP geometrical case of Figures 8 to 10, and defining β_1 as the bevelling angle of the brace wall-thickness (here assumed to be 45° deg), $z_{1.\beta}$ as the net brace-side of the weld region, p_1 as the bevelling penetration size (varying in the range: 3.00 to 6.00 mm for the case t_1=8.00 mm, and 6.00 to 12.00 mm for the case t_1=15.00 mm), and ψ_β as the post-bevelled dihedral angle at the root of the weld region, the throat-thickness efficiency factor distributions (χ_{at}) appear as

indicated in Figures 11 and 12, respectively for the case t_1=8.00 and 15.00 mm. It is interesting note that whichever geometric ratio $\beta=d_1/d_0$ and θ_1 is selected, the dihedral angle ψ along the welding path predominantly results in an obtuse angle (ψ>90), whereby a notable geometrical inefficiency of the FW solution is noted. For PJP solutions, however, χ_{at} is always able to ensure proper feasibility ($\chi_{at}\geq 0$), even for $\psi \rightarrow 150$°deg, which is a considerable level of efficiency.

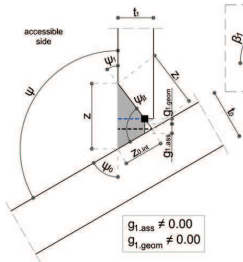

Figure 8. PJP, obtuse angle

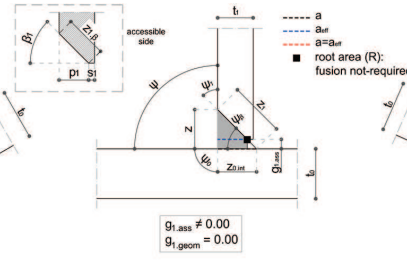

Figure 9. PJP, neutral angle

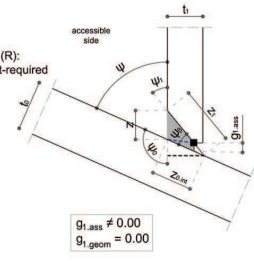

Figure 10. PJP, acute angle

Ultimately, when considering a cross-sectional overview of the χ_{at} parameter for FW (Figures 4 to 7) and PJP (Figures 11 and 12), it clearly highlights that the range $\psi\epsilon[30,90]$°deg can be defined as the maximum efficiency range, whereas for $\psi\epsilon[90,150]$°deg, a logical reduction of the weld efficiency is expected. It follows thus, that adequate balancing of the bead resistance along the circular path would lead to the necessity of butt/PJP and/or CJP, for at least obtuse dihedral angles.

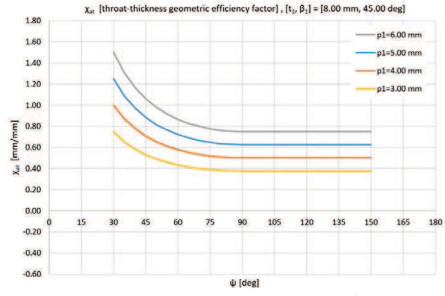

Figure 11. χ_{at} distribution (t_1=8.00, β_1=45.00)

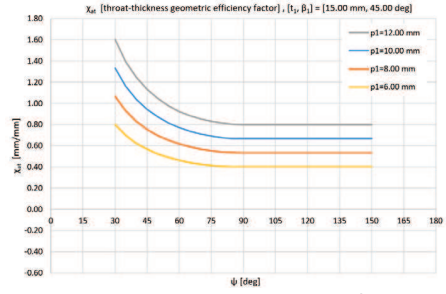

Figure 12. χ_{at} distribution (t_1=15.00, β_1=45.00)

3 Sample attainment according to EN9692, AS/NZS1554 and AWS-D1.1

In collaboration with CMM Laser, the current research applied for an experimental phase with the aim of obtaining 5 samples of CHS-to-CHS T-joints, with the PJP bevelling plane characterized by continuous variability of the post-bevelled dihedral angle (ψ_β). The 5 geometric samples are described in Figures 13 to 15. The geometric CAD input-files were developed in Catia (Dassault Systèmes) by the authors and the CAM application performed by CMM Laser with two types of LTC machine models. The expected bevelled region was interpolated by 3°deg polar sectors (Figure 16), with a continuous variability of the geometrical section; Figure 19 shows an exemplar section for the case ρ=30°deg. The chord element (CHS273*12.50 S355J2H) was obtained by making use of the LT24 model produced by Adige-sys (CO_2 laser system), while, with the more complex brace element connection (CHS168*8.00 S355J2H), a 3D FABRI GEAR 220 MK3 produced by Mazak Optonics Corp, was utilized (CO_2 laser source 4.00 kW, 6 axis-laser, diameter

range 20÷220 mm, maximum laser-beam inclination α_{ltc}=45°deg, maximum recommended allowable thickness t_{max}=20÷25 mm). Figure 18 shows a moment during the experimental phase.

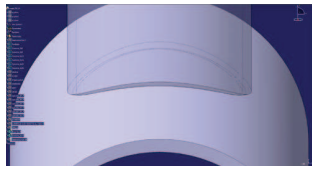

Figure 13. Catia model

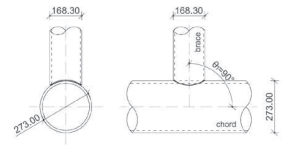

Figure 14. Sample geometry

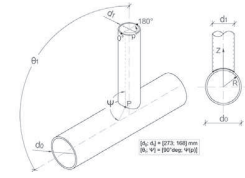

Figure 15. Reference systems

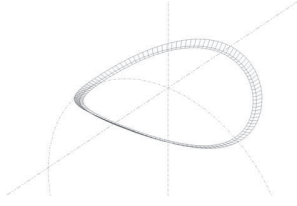

Figure 16. Weld 3D-region

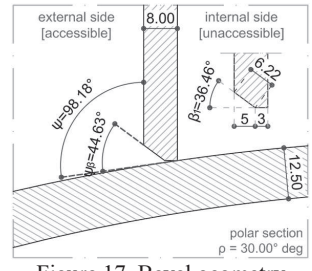

Figure 17. Bevel geometry

Figure 18. Experimental phase

Two of the five samples were analyzed and subjected to quality testing protocols at Code a Weld laboratories (Radstock Department, using a multi-purpose welding gauge in accordance to ISO EN 17637:2016, Figure 21) to verify the geometric accuracy of the bevelled region, and generally full conformity to EN9692, AS/NZS1554 and ASW-D1.1.

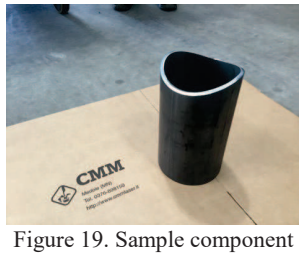

Figure 19. Sample component

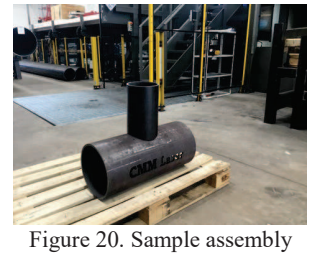

Figure 20. Sample assembly

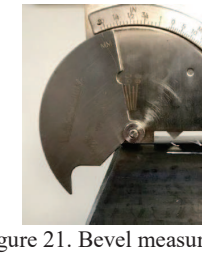

Figure 21. Bevel measurement

4 Fillet weld (FW) and partial joint penetration (PJP) solution in CHS-to-CHS joints: comparison in terms of stress and load distribution

At the recent XVI International Symposium of Tubular Structures, held in Melbourne, Chen, Ma and Wang (2017) of Tongji University presented the findings of their research. In their paper, an experimental process is described pertaining to the influence of NUSD (Non-Uniform Stress Distribution) on the failure mode of intersections of CHS-to-CHS X-joint. Then, in correlation to the geometry studied by Chen et al (2017), as well as the 5 samples described in the previous section, 2 finite element models were implemented: model_FW_01, characterized by an external fillet weld region z_0=7.50 mm, $z_1=z_0+[g_{1.ass}+g_{1.geom}(\rho)]$, and model_PJP_01, characterized by a butt weld region (PJP) with a_{eff}=5.00 mm. For both, the numerical sample was set t_0=25.00 mm,

to minimize the NUSD effect. Figures 22 and 23 show, for model_FW_01 and model_PJP_01, the welding geometrical properties z_0, a_{eff}, ψ, ψ_β and β_1. The CAD-geometry, created in Catia (Dassault Systemès), was imported into the latest version of Strand7®'s Nonlinear environment, by making use of the new R3 beta-version; Figures 24 (model_FW_01) and 25 (model_PJP_01).

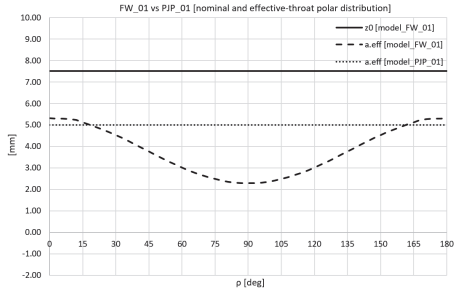

Figure 22. Throat polar-distribution (FW vs PJP)

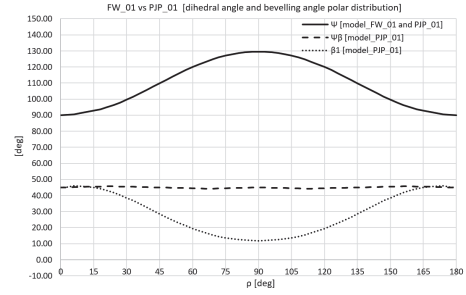

Figure 23. Dihedral/bevel polar-distribution (PJP)

The package was integrated by the version 3.0.0 of the Application Programming Interface (API), which was used to manage the interface between the geometric environment (CAD), and the mechanical environment problem (FEM). More details pertaining to the mesh generation, materials, parametric entries, restraints and loading conditions can be found in Mastropasqua (2019). The numerical samples were restrained in accordance to Figure 24, which perfectly correlated to the loading tests conducted at Tongji University (Chen et al, 2017). The loading was characterized by a parametric through-thickness distributed load of 1.00 kN (0.25 kN for each 90°deg angular sector, due to the symmetry), which was incremented, and ranged from: 0➔1000 kN. The numeric response highlighted some interesting - albeit not unexpected - points: in the loading-sector 1 (0÷500 kN, FW_elastic/PJP_elastic), the expected bell-shaped curve is evident for the FW and PJP, with the accentuation of the well-known ZZ-stress level at the saddle point.

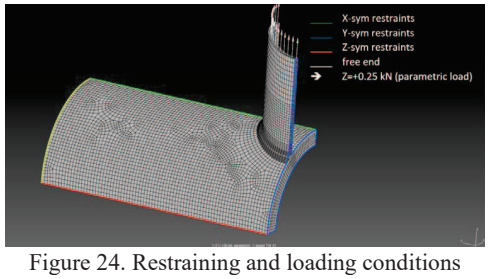

Figure 24. Restraining and loading conditions

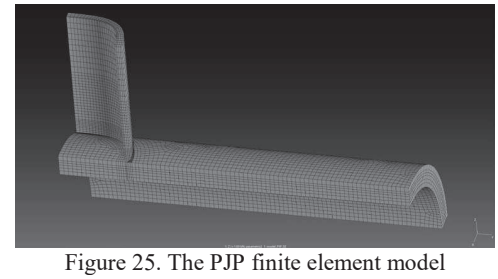

Figure 25. The PJP finite element model

Although, on closer inspection of the curves, a more regular distribution of the PJP solution is evident, whereas for the FW curves, it indicates a more prominent ZZ-stress factor around ρ≈70°and 110°deg. The observation is also confirmed by a slight VM-stress reduction in the same polar angular sectors. This second observation on the FW response, is dependent on a specific NUSD distribution and a superimposed non-uniform spatial variation of the throat-plane angle. Figures 26 and 27 show a comparison of ZZ-stress and VM-stress for the two samples. In loading-sector 2 (500÷700 kN, FW_plastic/PJP_elastic) it shows that for a FW, a widening of the plastic angular sector from the saddle point (ρ=90°deg) to $\rho_{plastic}$=45|135°deg occurs. In the PJP model, however, a quasi-proportional increment of the stress level is noted, with the exception of the level N_{Ed}=+700 kN, where the beginning of the plastic-flattening is observed at the saddle point.

However, although this is a local effect, the overall response of the full weld-region can be nominally considered as still being elastic. Figures 28 and 29 can help to better understand the incremental response of the two throat-regions in the loading range 0÷1000 kN for several angular sectors. Sector 3 (700÷1000 kN, FW_plastic/PJP_plastic) leads the plastic angular sector from/to $\rho_{plastic}$=15|165°deg for both models; FW and PJP.

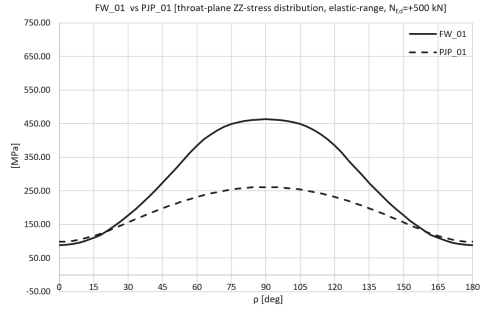

Figure 26. ZZ-stress @ N_{Ed}=500 kN

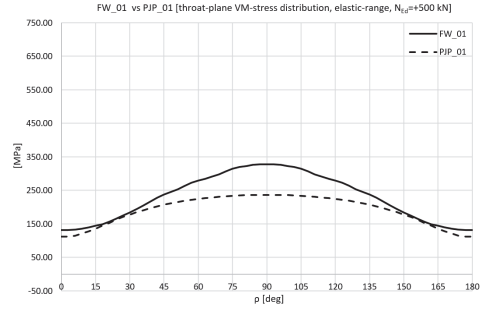

Figure 27. VM-stress @ N_{Ed}=500 kN

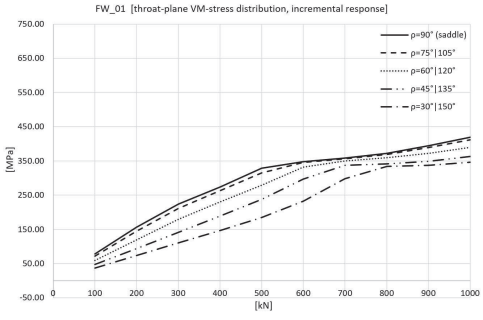

Figure 28. VM-stress incremental response (FW)

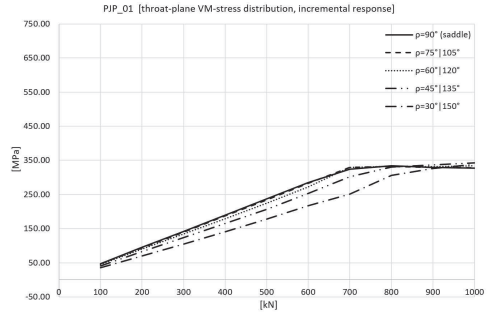

Figure 29. VM-stress incremental response (PJP)

Lastly, in addition to the qualitative remarks noted, a quantitative interpretation of the curves emphasizes a reasonable difference between ZZ and VM-stress (Figure 30 and 31) concerning the FW and PJP models.

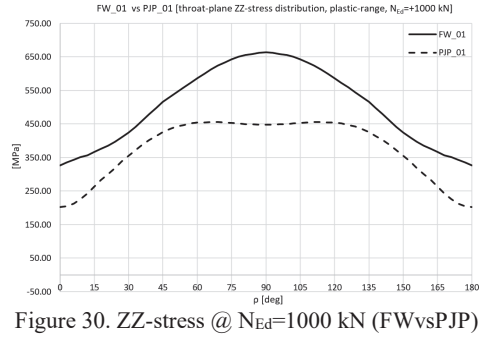

Figure 30. ZZ-stress @ N_{Ed}=1000 kN (FWvsPJP)

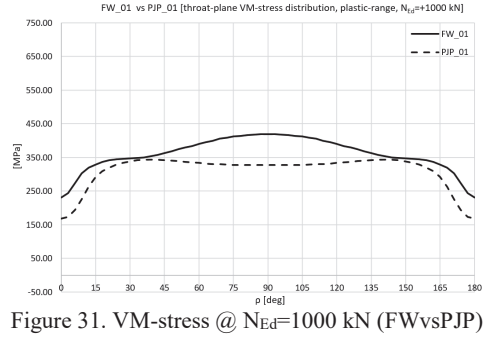

Figure 31. VM-stress @ N_{Ed}=1000 kN (FWvsPJP)

5 Conclusions: final considerations on the mechanical response of PJP solutions

Five CHS-to-CHS T-joint samples were obtained during an experimental phase by means of one of the latest machines produced by Mazak Optonics Corp, a CO_2 6 axis-system with laser-head inclination α_{ltc}=45°deg. The end-bevelled surface results were characterized by continuous variability of the post-bevelled dihedral angle (ψ_β), with full conformity to the welding codes EN9692, AS/NZS1554 and ASW-D1.1. The geometric samples were studied by making use of non-linear finite element simulations. Interpretation of the results showed that although the shape and magnitude of the local deformation of the chord appeared indeed unaffected, the PJP solutions shows a more favourable brace-axial (ZZ) and Von Mises (VM) stress distribution through the throat-plane. Two fundamental factors are behind this important finding: the different effective-throat width distribution a_{eff}=$a_{eff}(\rho)$ and the different throat-plane inclination with reference to the external ZZ load. It is clear that both the factors are strictly related to the polar variability of the welding region due to the dihedral angle (Ψ); comparing the FW with the PJP solution, in terms of the stress, the bevelled solution shows a significant quantifiable reduction of the stress intensity as the polar angle (ρ) approaches to the saddle point of the intersection. The PJP solution, due to the continuous orthogonality of the throat plane (TP) to the external ZZ-load, shows a more regular variation of the VM component, which is always closely fitted to the ZZ-curve. During the post-elastic response, both systems show a progressive extension of the plastic redistribution, but, due to the considerable reduction of the TP width of the FW in the proximity of the saddle point, the overall external ZZ-load carried by the weld region is logically less than what is observed for the PJP case. As a consequence, the PJP solution shows a regular flat-distribution of the external load, whereas the FW tends to decentralize the area of the load transmission toward the crown regions due to the throat-plane size enhancements. It follows that, whichever parameter is adopted to establish the ultimate strength of the connection (VM stress and/or strain deformation) the PJP solution is capable of providing a considerably higher strength.

References

CEN 2005, *Welding and allied processes - Recommendations for joint preparation*, Part 1: Manual metal-arc welding, gas-shielded metal-arc welding, gas welding, TIG welding and beam welding of steel and Part 2: Submerged arc welding of steel. EN ISO 9692-1:2013 and 9692-2:2001, Brussels.

AS/NZS1554.1:2014, *Structural steel welding - Welding of steel structures*, Technical committee WD-003, Australian/NewZealand Standard

AWS D1.1/D1M: 2015, *Structural welding code - Steel*, American Welding Society, 2015

Mastropasqua A, *Laser Tube Cutting - Stress distribution in CHS-to-CHS joints welded by partial joint penetration (PJP) according to the most recent fabrication codes EN1090 (european), AS/NZS5131 (australian/newzealand) and AISC303 (american)*. Ph.D. Thesis, Faculty of Engineering Technology, EGS University, Paris, 2019

ISO EN 17637:2016, *Non-destructive testing of welds - Visual testing of fusion-welded joints*, International Organization for Standardization, Geneva, 2016

Chen YY, Ma X, Wang W, *Non-uniform stress distribution at weld of CHS-CHS joint and its effect on failure mode,* Tubular Structures XVI, Proceedings of 16th Int. Symp. on Tub. Structures, ISTS16, Melbourne, 2017

Strand7 Software, *API Manual* - Documentation for the Strand7 Application Programming Interface, R3 β-version 2019, Strand7 Pty Limited, Sydney, 2019